Volume 20, No 2 | International Journal of Radiation Research, April 2022

Dynamic contrast enhanced MRI Pharmacokinetic parameter histogram analysis in diagnosis of malignant prostatic lesions

X.M. Ma[#], L.L. Wang[#], P. Wang, Y.Q. Ma, We.W. Zhang, J.W. He, G. Huang[*], L.P. Zhao[*], J.L. Ren, Z.Q. Shi

Radiology Department, Gansu Provincial hospital, Donggang West Road, Lanzhou, Gansu Province, China 730000

► ***Original article***

***Corresponding author:**
Dr. Gang Huang
E-mail: *knee0999@163.com*
Dr. Lian-ping Zhao,
E-mail:
lianping_zhao007@163.com

Received: January 2021
Final revised: September 2021
Accepted: October 2021

Int. J. Radiat. Res., April 2022; 20(2): 491-498

DOI: 10.52547/ijrr.20.2.34

[#]These authors contributed equally to this work.

Keywords: *Histogram, pharmacokinetic parameters, dynamic contrast-enhanced MRI, prostate cancer, benign prostatic hyperplasia.*

ABSTRACT

Background: To differentiate prostate cancer and benignprostatichyperplasia by WAHPP (the whole lesion histogram analysis of the pharmacokineticparameters) of dynamic contrast-enhancedMRI (DCE-MRI). ***Materials and Methods***: Totally 62 patients with elevated prostate specific antigen (PSA) (> 4 ng/ml) were grouped as prostate cancer (PCa) group (n=33) and benign prostatic hyperplasia (BPH) group (n=29) based on transrectal ultrasound (TRUS)-guided random biopsy diagnosis and their WAHPP- K^{trans} (constant is transferred from the blood plasma to the extracellular extravascular (EE) space), K_{ep} (back into blood plasma at a steady rate from EE space), V_e (EE volume fraction) and V_p (fractional blood plasma volume) were compared. ***Results***: WHAPP shows the 5th percentile and entropy of K^{trans}, $5^{th}/10^{th}/25^{th}/50^{th}/75^{th}/90^{th}/95^{th}$ percentiles, mean value and entropy of K_{ep}, 5^{th} percentile and uniformity of V_e, $5^{th}/10^{th}/25^{th}/50^{th}/75^{th}$ percentiles, V_p had a considerably greater mean value and entropy in PCa than in BPH (p0.05). The 90th percentile of Kep's maximum AUC (area under the curve) was 0.764, according to receiver operating characteristic (ROC) study, the Youden index 0.5507, the sensitivity 75.76%, and the specificity 79.31%. ***Conclusion***: K^{trans}, K_{ep}, and V_e of WHAPP canbe used to quantify prostate DCE-MRI. The 90^{th} percentile of K_{ep} possibly will be the best indicator for the differential diagnosis of malignant and BPH.

INTRODUCTION

Prostate cancer (PCa) is one of the commonest malignant cancer in the male reproductive system; the disease is increasing year by year in China, and the incidence rate is only lower than that of lung cancer and colorectal cancer [(1)]. Prostate specific antigen (PSA) as one of the most effective clinical biomarker has been widely used to screen for prostate cancer. However, the specificity of PSA alone is not satisfactory, especially in the so-called PSA grey area, which has a specificity of only 25-40% [(2)]. This can lead to unnecessary treatment and increase potential health risks and medical expenses. Furthermore, the most common urinary system disease in older men is benign prostatic hyperplasia (BPH) [(3)]. Although the clinical signs and symptoms of PCa and BPH are similar, the treatment and prognosis are quite different; therefore, accurate preoperative assessment is very important for the patients' treatment plan [(4)].

Clinically, the simultaneous presence of benign and malignant disease is observed quite often (83.3%) and the clinical treatment decisions were consistent regardless of whether prostate cancer patients were associated with BPH or not [(5,6)]. At present, the diagnosis of benign and malignant prostate lesions in patients with elevated PSA is mainly dependent on ultrasound-guided puncture biopsy. Because biopsy is an invasive examination, patients are poorly tolerated, it can bring great psychological burden to patients, and previous studies have showed that to perform a biopsy only based on elevated PSA can led to the increase of unnecessary biopsies (up to 75%) [(7)]. Therefore, evaluating the biological aggressiveness of prostate lesions non-invasively is of great clinical importance.

Magnetic resonance imaging (MRI) with its high soft tissue resolution, arbitrary plane and multi-parameter imaging, without ionizing radiation, etc., has been widely used in the preoperative diagnosis of prostate diseases [(1)]. Conventional T1 and T2 weighted imaging are often used for localizing and staging prostate cancer, but their diagnostic efficiency is low, which cannot meet the demand of clinical requirement. Currently, T1 and T2 weighted images are more often just used as an auxiliary tool, mainly for providing location information before TRUS guided biopsy [(8)].

[DOI: 10.52547/ijrr.20.2.34]

With the recent development of MRI techniques, functional imaging, dynamic contrast-enhanced MRI (DCE-MRI) and MRspectroscopy (MRS), has become a good way to rule out high-risk PCa lesions. It can be used as an auxiliary test for biopsy with PSA [9-11]. Among these techniques, DCE-MRI has gained more and more attention for its value in the diagnosis of early stage PCa noninvasively because it can aid in the interpretation of T2W MRI and diffusion weighted imaging (DWI) in the diagnosis of high-risk prostate cancer and the status of postprostatectomy, radiation, or focused ablation [12]. Previous studies usually use the average of pharmacokinetic parameters (PKPs) to judge the perfusion lesions. The cell density and vasculature structures are markedly heterogeneous in the major tumors, resulting in radiologic heterogeneity [13]. A large number of studies have attempted to extract heterogeneity indicators from regions of interest (ROI) using WAHPP (the whole lesion histogram analysis of the pharmacokinetic parameters) to reveal various biological characteristics of tumors and enhance diagnostic abilities [14-16]. However, there are few reports on prostate cancer DCE-MRI using WAHPP.

The goal of this study is to differentiate Pca from BPH by using WAHPP of DCE-MRI and demonstrate that the values of K^{trans} (constant is transferred from the blood plasma to EE space), K_{ep} (back into blood plasma at a steady rate from EE space), V_e (extracellular extravascular volume fraction) and V_p (fractional blood plasma volume) were considerably increased in PCa than in patients with BPH.

MATERIALS AND METHODS

Patients

The institutional review board of the Institute of Clinical Medicine, Gansu Provincial Hospital (No. 2016–089) authorized this retrospective study on December 13, 2016. Between January 2014 to January 2017, 122 patients with PSA>4 ng/ml were referred for prostate MRI before biopsy from the department of urology at Gansu Provincial Hospital. The inclusion criteria were: (a) age between 40 and 75 years; (b) no evidence of PSA increase by noncancerous factors, such as urinary infection, prostatitis, bladder stones or previous prostate biopsy. Of these patients, 60 patients were excluded because of: (a) urinary infection, prostatitis, bladder stones or previous prostate biopsy (n=7); (b) DCE-MRI not performed because of poor health (n=6); (c) underwent previous treatment including hormone therapy or radiation (n=12); (d) imaging with artifacts, rendering the examination no diagnostic (n = 17); (e) no biopsy 6 weeks (n=18). Standard 12-core TRUS-guided random biopsy using 18-gauge biopsy cut needles was performed in all patients by two experienced urologists (8 and 15 years of experience at the start of this study, respectively). The urologists were blinded to the MRI results before TRUS-guided random biopsy. Finally, the study included 62 patients with a mean age of (60.66±13.38) years (range 41-87years). Of these 62 subjects, 33 patients were diagnosed with Pca (containing patients with cancer presenting in the prostate with BPH) with a Gleason score of 3+3 and above, and the other 29 patients were diagnosed with BPH (figure 1).

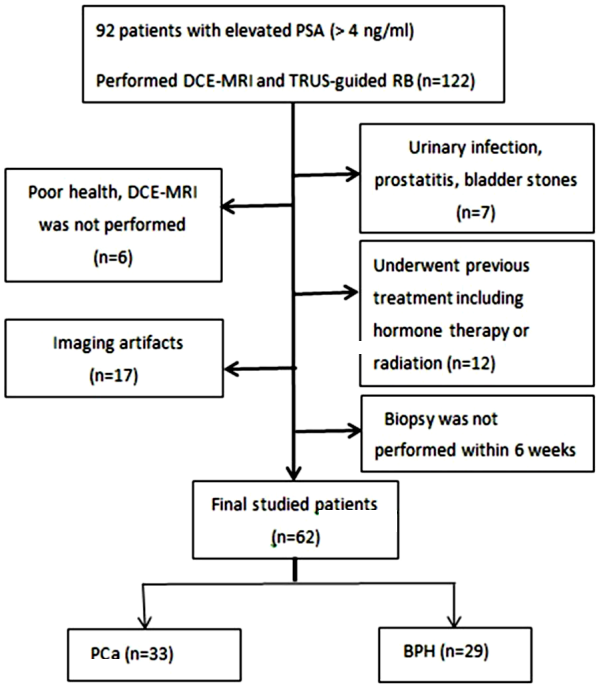

Figure1. Flowchart of patient selection.

MRI techniques

All MRI studies were performed with a 3.0-T MRI system (Magnetom skyra; Siemens Healthcare, Erlangen, Germany) equipped with an 18-channel phased-array body coil. All patients underwent Multiparametric MRI (mp-MRI) examinations including transverse T1-weighed imaging, triplanarT2-weighted turbo4spin echo imaging, DW-MRI and DCE-MRI. The sequence parameters are listed in table 1. DCE-MRI contained 35 scans of about 8 second each. T1 mapping was performed using a total of 2 flip angles (FAs) (2° and 15°) and 3-dimensional spoiled gradient recalled echo sequences for the contrast agent concentration conversion. Two pre-contrast phases were obtained before bolus injection, and then Gd-DTPA (Omniscan; GE Healthcare Co., Ltd., Shanghai, China) was administered in a dose of 0.1 mmol/kg with a venous cannula for flow rate of3 ml/sec followed by a 20 ml saline flush.

[DOI: 10.52547/ijrr.20.2.34]

Figure 1. Modified Ondo Google Satellite Map Showing Zones of Sample Collection. Map data ©2017 Google (14)

	TR/TE	Slice thickness/Layer space, mm	Acquisition matrix	FOV, mm	Scan time	Sequence
Axial T1WI	600/18	4/0.8	448x70%	28x28	1'56	TSE
Axial T2WI	4020/68	4/0.8	448x75%	28x28	2'45	FS-TSE
Coronal T2WI	4020/68	4/0.8	448x75%	28x35	1'45	TSE
Sagital T2WI	4020/68	4/0.8	384x80%	28x28	1'45	TSE
Axial DWI	4400/85	4/0.8	192x85%	28x28	1'50	EPSE,b=0,800 s/mm2
DCE-MRI	5.08/1.77	3.6/0	192x80%	28x28	4'44	T1 VIBE;20 Slice/ phase;total 35 phases

MRI Image Post processing

The DCE-MRI images were analyzed blindly by 2 radiologists (with 5 and 8 years of experience with abdominal MRI, respectively) by DCE-MRI quantitative software package (Omni-Kinetics, GE Healthcare). Tumors were segmented by plotting a series of regions of ROIs at successive levels for each lesion at the most enhanced phase, covering the whole tumor where possible, but excluding vessels, necrosis, cystic-appearing areas and calcifications by referring to other sequence images. The PKPs were analyzed based on the Extended Tofts model. The arterial input function (AIF), an estimation of the concentration-time profile of the tracer in a nearby vessel, was obtained by placing a ROI on the abdominal aorta. The parameters of $K^{trans,}$ K_{ep}, V_e and V_p were generated for each voxelwise ROIs defined values. Various histogram metrics including mean value, $5^{th}/10^{th}/25^{th}/50^{th}/75^{th}/90^{th}/95^{th}$ percentiles, skewness, kurtosis, energy, entropy and uniformity were calculated from the lesion segmentation.

Pathologic assay

The prostate tissue was positioned on a slide after being embedded in paraffin, then all slices were stained with hematoxylin-eosin and scanned using the AperioSlide Scanning System (Scan Scope T3; Aperio Technologies Inc., Vista, CA, USA) for high-resolution digital images (0.25 lm/pixel at 40) and they were interpreted by 2 experienced pathologists jointly with virtual slides using Image Scope viewing software (Aperio Technologies, Inc.) and ahigh-resolution monitor. The time interval between mpMRI and biopsy was in 1 month, with a mean of 8 days.

Statistical analysis

SPSS 19.0 (IBM, NY, USA) or MedCalc 15.8 (MedCalc, Mariakerke, Belgium) were used for all statistical analyses. After testing the normal distribution with the Kolmogorov-Smirnov test, *t* test or Wilcoxon–Mann–Whitney test were used to compare PKPs between benign and malignant prostate lesions. Receiver operating characteristic (ROC) curves analysis was used to evaluate the differential diagnostic performance of DCE-MRI histogram metrics for PCa and BPH. A multivariate logistic regression method was used to develop a multi-metirc discriminant model to improve efficiency. The optimal sensitivity and specificity of each histogram-derived PKPs were calculated based on the Youden index (YI). $P < 0.05$ indicated statistically significant.

RESULTS

Patient demographics and histopathological findings

Of total 62 patients, there were 33 PCa (53.2%) and 29 BPH (46.8%) according to TRUS-guided biopsy. The mean age of PCa group was 72 years (range 60-88) while the average age of BPH group was 71 years (range 60-85), which has no statistical significance ($P > 0.05$).

Comparison of histogram parameters between PCa and BPH

The 5^{th} percentile and entropy values of K^{trans}, the $5^{th}/10^{th}/25^{th}/50^{th}/75^{th}/90^{th}/95^{th}$ percentiles, mean value and entropy of K_{ep}, the 5^{th} percentile and uniformity of V_e, $5^{th}/10^{th}/25^{th}/50^{th}/75^{th}$ percentiles, mean value and entropy of V_p were significantly higher in Pca than in BPH ($p<0.05$), and the kurtosis and energy of K^{trans}, skewness and kurtosis of K_{ep} and V_p were considerably lower in Pca than in BPH ($P<0.05$; table 2; figures 3-5).

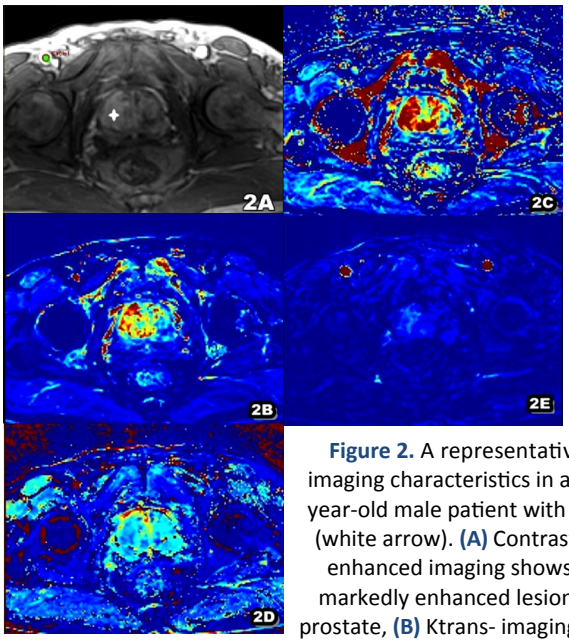

Figure 2. A representative imaging characteristics in a 69-year-old male patient with PCa (white arrow). **(A)** Contrasted enhanced imaging shows a markedly enhanced lesion in prostate, **(B)** Ktrans- imaging. **(C)** Kep imaging. **(D)** Ve imaging. **(E)** Vp imaging.

[DOI: 10.52547/ijrr.20.2.34]

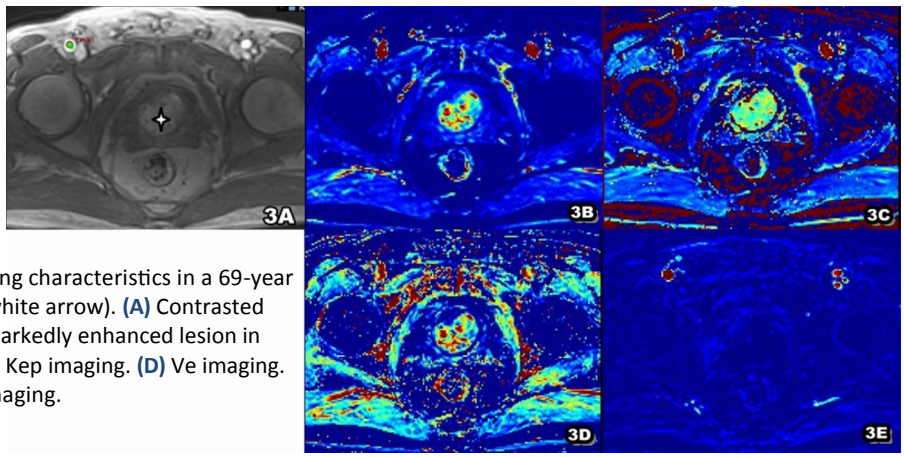

Figure 3. A representative imaging characteristics in a 69-year -old male patient with BPH (white arrow). **(A)** Contrasted enhanced imaging shows a markedly enhanced lesion in prostate. **(B)** Ktrans imaging. **(C)** Kep imaging. **(D)** Ve imaging. **(E)** Vp imaging.

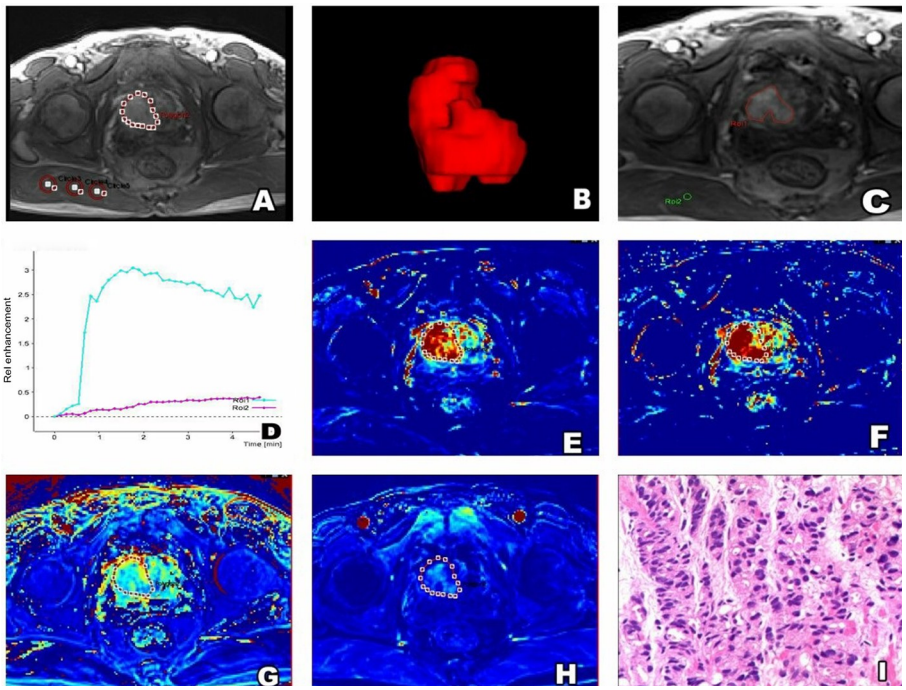

Figure 4. Showing the same patient with prostate cancer in figure 2. **(A)** polygon 2 in prostate shows edge of the lesion that we have outlined , circle 3-5 shows the ROI of normal tissue, (B) is the 3D-ROI of the lesion, **(C)** ROI1 represents normal tissue and ROI2 represents lesion. **(D)** is the DCE-TIC of ROI1 and ROI2, **(E-H)** shows the ROI of lesion copied from A in Ktrans-imaging, kep-imaging, Ve-imaging and Vp-imaging. **(I)** is the pathological picture of the patient (HE×100).

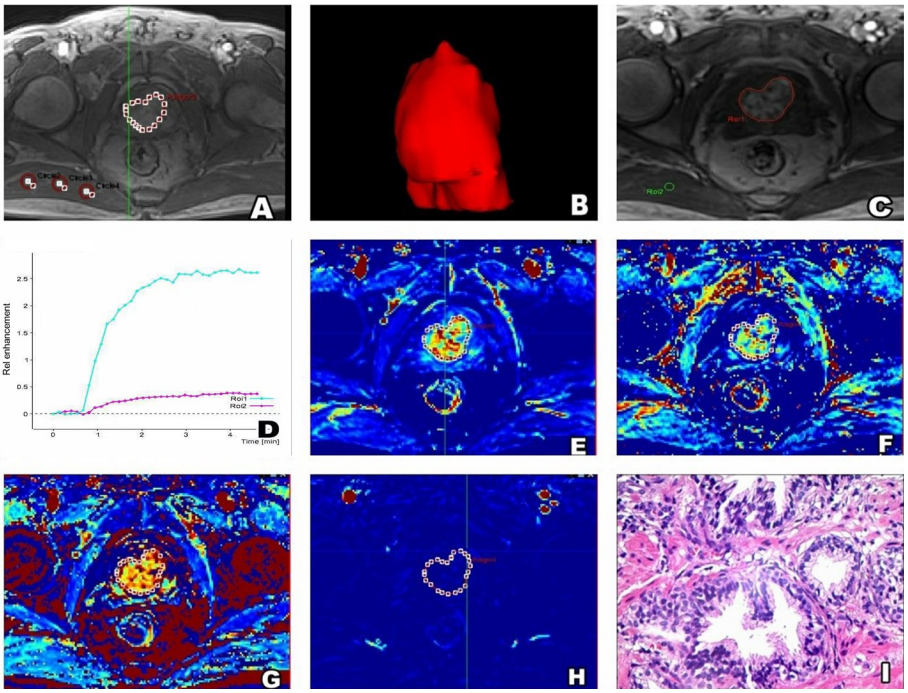

Figure 5. Showing the same patient with prostate hyperplasia in figure 3. **(A)** polygon 2 in prostate shows edge of the lesion that we have outlined , circle 3-5 shows the ROI of normal tissue, **(B)** is the 3D-ROI of the lesion, **(C)** ROI1 represents normal tissue and ROI2 represents lesion. **(D)** is the DCE-TIC of ROI1 and ROI2, **(E-H)** shows the ROI of lesion copied from A in Ktrans-imaging, kep-imaging, Ve-imaging and Vp-imaging. **(I)** is the pathological picture of the patient (HE×100).

[DOI: 10.52547/ijrr.20.2.34]

Table 2. Comparison of histogram parameters between PCa and BPH (mean ± SD).

Variables	Significance test		
	Benign lesions (n=33)	Malignant lesions (n=29)	P-value
Histogram K^{trans}			
5th(min-1)	0.048±0.044	1.820±9.913	0.049
10th(min-1)	0.073±0.057	1.978±10.631	0.112
25th(min-1)	0.122±0.089	2.406±12.687	0.122
50th(min-1)	0.195±0.139	2.872±14.768	0.126
75th(min-1)	0.297±0.213	3.307±16.462	0.173
90th(min-1)	0.422±0.315	3.742±18.006	0.129
95th(min-1)	0.518±0.408	3.947±18.530	0.144
MeanValue	0.229±0.166	2.873±14.551	0.179
skewness	1.622±0.910	1.200±0.70	0.084
kurtosis	6.601±8.427	2.531±3.210	0.008
Energy	0.014±0.005	0.012±0.006	0.035
Entropy	6.508±0.479	6.812±0.444	0.015
uniformity	0.338±0.163	0.379±0.200	0.212
Histogram K_{ep}			
Quantile 5	0.065±0.100	0.207±0.149	0.001
Quantile 10	0.141±0.125	0.301±0.187	0.001
Quantile 25	0.315±0.152	0.504±0.263	0.001
Quantile 50	0.542±0.190	0.820±0.354	0.001
Quantile 75	0.814±0.267	1.242±0.498	0.001
Quantile 90	1.137±0.415	1.738±0.696	0.000
Quantile 95	1.389±0.565	2.080±0.841	0.001
MeanValue	0.610±0.228	0.935±0.379	0.001
Skewness	1.695±0.093	1.158±0.703	0.730
kurtosis	10.530±8.638	2.482±3.560	0.137
Energy	0.019±0.012	0.019±0.022	0.008
Entropy	6.477±0.569	6.796±0.491	0.024
uniformity	0.261±0.210	0.329±0.18	0.212
Histogram V_e			
5th(min-1)	0.056±0.081	0.140±0.134	0.045
10th(min-1)	0.146±0.123	0.171±0.152	0.732
25th(min-1)	0.228±0.148	0.236±0.198	0.742
50th(min-1)	0.321±0.195	0.329±0.248	0.783
75th(min-1)	0.403±0.234	0.429±0.312	0.930
90th(min-1)	0.488±0.257	0.506±0.379	0.909
95th(min-1)	0.553±0.265	0.559±0.425	0.682
MeanValue	0.352±0.203	0.380±0.283	0.030
Skewness	1.938±0.497	1.894±3.650	0.084
Kurtosis	14.406±24.861	29.854±62.422	0.298
Energy	0.023±0.018	0.036±0.054	0.541
Entropy	6.397±0.790	6.086±0.868	0.409
Uniformity	0.383±0.305	0.544±0.294	0.003
Histogram V_p			
5th(min-1)	0.00006±0.000054	0.00024±0.00047	0.008
10th(min-1)	0.00010±0.000109	0.00099±0.0032	0.007
25th(min-1)	0.00027±0.00027	0.00552±0.0157	0.006
50th(min-1)	0.0015±0.00206	0.020±0.044	0.003
75th(min-1)	0.011±0.011	0.0480±0.089	0.018
90th(min-1)	0.026±0.019	0.079±0.130	0.054
95th(min-1)	0.036±0.025	0.100±0.152	0.066
MeanValue	0.008±0.006	0.032±0.056	0.017
Skewness	3.515±2.76	2.582±1.935	0.041
Kurtosis	27.405±18.091	12.553±19.893	0.046
Energy	0.407±0.207	0.253±0.232	0.002
Entropy	3.398±1.332	4.574±1.744	0.004
Uniformity	-1.267±1.323	-0.763±1.069	0.011

Calculated of time intensity curve (TIC) for the lesion tissue

The calculated time Intensity Curve (TIC) curve of lesion tissue showed that the enhancement rate of both prostate cancer tissue and BPH tissue was increased rapidly about 80 seconds after the injection of contrast agent, with a higher contrast in the normal tissue (figures 4 and 5). Then, the tumors were segmented by drawing a series of ROIs on the continuous levels for each lesion in the most enhanced phase (phase 10 or 11), covering the whole tumor where possible but excluding visible necrosis, vessels, cystic-appearing areas and calcifications by referring to the scope of the lesion in ultrasound-guided biopsy and other sequence images (figures 4A and 5A), then the ROI was copied to the corresponding penetration parameter diagram (Figures 4E-4H and 5E-5H)), the ROIs of region in every slice were merged into a 3D-ROI (Figures 4B and 5B).

ROC analysis of histogram metrics

The ROC results for each histogram-derived indicator were used to discriminate between malignant and benign prostatic lesion were presented in table 3: the kurtosis of K^{trans}-highest AUC value was of 0.698(0.566-0.830), YI of 0.365, sensitivity and specificity of 69.8% and 57.6%, respectively. The 90th percentile of K_{ep} -highest AUC was of 0.724 (0.241-0.966), YI of 0.551, sensitivity specificity of 76.4% and 69.7%, respectively. The uniformity of V_e-highest AUC value was of 0.655 (0.207-0.862), YI of 0.387, sensitivity specificity of 69.9% and 66.7%, respectively. However, the energy of V_p showed the highest AUC value of 0.931 (0.655-1.000) with a 0.420 YI, sensitivity was 72.9% and specificity was 42.4 %.

Multivariate logistic regression analysis of the histogram metrics

Multivariate logistic regression analysis showed that AUCs of overall histogram metrics of K^{trans}, K_{ep}, V_e and V_p were 0.893 (95% CI, 0.826-0.947), 0.900 (95% CI, 0.837-0.955), 0.867 (95% CI, 0.769-0.922), 0.861 (95% CI, 0.798-0.923), respectively (figure 6).

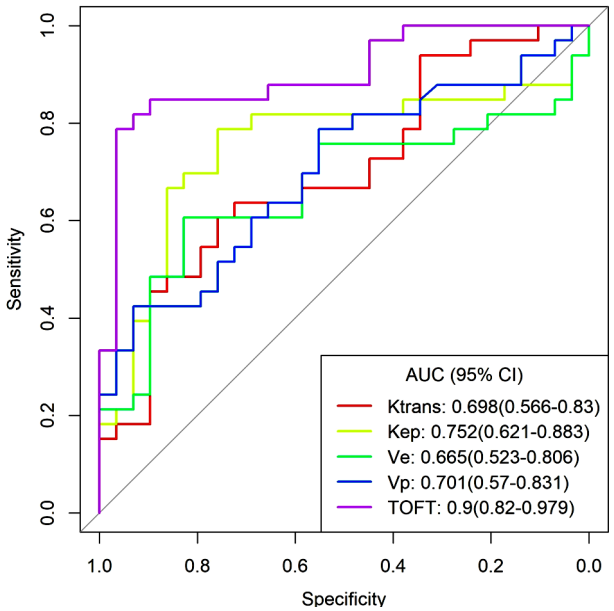

Figure 6. Receiver Operating Characteristic (ROC) curves of K^{trans}, K_{ep}, Ve and V_p, illustrating the performance of the statistically significant difference parameters when distinguishing PCa from BPH.

[DOI: 10.52547/ijrr.20.2.34]

Table 3. ROC analysis of histogram-derived parameters in differentiating malignant from benign prostate lesions.

Variables	Sensitivity (%)	Specificity (%)	AUC	Youden index	Cutoff value
Histogram K^{trans}					
5th(min-1)	63.64	68.97	0.646	0.326	0.0464053
10th(min-1)	60.61	68.97	0.618	0.2957	0.0632157
25th(min-1)	60.61	72.41	0.614	0.3302	0.111483
50th(min-1)	63.64	65.52	0.613	0.2915	0.172669
75th(min-1)	72.73	51.72	0.601	0.2445	0.224641
90th(min-1)	45.45	75.86	0.612	0.2132	0.600943
95th(min-1)	48.48	75.86	0.608	0.2435	0.729246
Mean Value	60.61	62.07	0.6	0.2268	0.195493
Skewness	63.64	65.52	0.628	0.2915	1.10853
Kurtosis	60.61	75.86	0.698	0.3647	1.66993
Energy	48.48	86.21	0.656	0.3469	0.00943243
Entropy	51.52	86.21	0.68	0.3772	6.90119
Uniformity	36.36	93.1	0.592	0.2947	0.475887
Histogram K_{ep}					
Quantile 5	78.79	75.86	0.752	0.5465	0.0802911
Quantile 10	81.82	68.97	0.747	0.5078	0.144737
Quantile 25	69.7	82.76	0.747	0.5246	0.395404
Quantile 50	75.76	82.76	0.75	0.5852	0.627301
Quantile 75	69.7	82.76	0.758	0.5246	0.95783
Quantile 90	75.76	79.31	0.764	0.5507	1.21596
Quantile 95	72.73	75.86	0.754	0.4859	1.52207
Mean Value	72.73	79.31	0.754	0.5204	0.662814
Skewness	84.85	34.48	0.526	0.1933	1.61761
Kurtosis	81.82	37.93	0.61	0.1975	3.52379
Energy	63.64	82.76	0.696	0.4639	0.0112198
Entropy	72.73	62.07	0.667	0.348	6.64813
Uniformity	42.42	89.66	0.592	0.3208	0.416625
Histogram V_e					
5th(min-1)	60.61	82.76	0.665	0.4336	0.0839478
10th(min-1)	36.36	79.31	0.527	0.1567	0.220273
25th(min-1)	51.52	62.07	0.526	0.1358	0.163323
50th(min-1)	63.64	48.28	0.522	0.1191	0.323242
75th(min-1)	18.18	93.1	0.501	0.1129	0.731027
90th(min-1)	39.39	72.41	0.515	0.1181	0.303803
95th(min-1)	48.48	68.97	0.538	0.1745	0.447238
Mean Value	42.42	72.41	0.513	0.1484	0.216835
Skewness	51.52	62.07	0.51	0.1358	0.960908
Kurtosis	45.45	68.97	0.554	0.1442	9.80086
Energy	66.67	48.28	0.546	0.1494	0.0150516
Entropy	63.64	62.07	0.599	0.2571	6.35746
Uniformity	69.7	68.97	0.699	0.3866	0.521587
Histogram V_p					
5th(min-1)	42.42	93.1	0.696	0.3553	0.000104952
10th(min-1)	42.42	93.1	0.701	0.3553	0.000209903
25th(min-1)	42.42	93.1	0.703	0.3553	0.000524759
50th(min-1)	51.52	89.66	0.717	0.4117	0.00368001
75th(min-1)	51.52	82.76	0.678	0.3427	0.0162758
90th(min-1)	39.39	89.66	0.643	0.2905	0.0449458
95th(min-1)	27.27	100	0.636	0.2727	0.0893808
Mean Value	36.36	96.55	0.676	0.3292	0.0186859
Skewness	45.45	89.66	0.651	0.3511	1.55956
Kurtosis	45.45	89.66	0.648	0.3511	2.55465
Energy	45.45	96.55	0.729	0.4201	0.126708
Entropy	54.55	79.31	0.712	0.3386	4.48284
Uniformity	42.42	93.1	0.689	0.3553	0.259359

Table 4. ROC analysis of combined histogram analysis.

Characteristics	AUC	p value	0.95 confidence interval
Overall K^{trans} HA	0.893	<0.0001	0.826-0.947
Overall K_{ep} HA	0.900	<0.0001	0.837-0.955
Overall V_e HA	0.867	<0.0001	0.769-0.922
Overall V_p HA	0.861	<0.0001	0.798-0.923

AUC, area under the receiver operating characteristic curve. HA, Histogram analysis.

DISCUSSION

PCa-DCE-MRI showed earlier and enhanced enhancement, flushing contrast agents significantly faster than normal or benign prostate tissue [17-19]. Our results showed that histogram metrics of quantitative DCE-MRI parameters of K^{trans}, K_{ep}, V_e and V_p were significantly different between PCa and BPH. This enhanced pattern is associated with tumor angiogenesis, as malignant tumor angiogenesis increases, and its up-regulated molecular pathway increases vascular permeability factor or vascular endothelial growth factor production and release. These newly formed blood vessels have a higher permeability than normal blood vessels because the integrity of the blood vessel wall is weak [20-21]. Our result indicated that V_e represented the EE space per unit volume of tissue; malignant tumors generally exhibited a lower V_e than the benign lesions because of higher cell density of malignant tumors. In general, malignant tumor vessels are more abundant and permeable than benign ones that lead to the higher K^{trans}, K_{ep} and V_p [22-23].

However, only 5th percentile of V_e was marginally significantly higher in malignant PCa in our study, which may be caused by the relatively small sample size. K^{trans} is more widely used to identify prostate lesion types. However, it can be affected by fluctuations in cardiac output and high blood pressure. However, the K_{ep} is relatively independent, while the AUC is the highest, with sensitivity and specificity of 75.76% and 79.31%, respectively. Therefore, it is not excluded that the 90th percentile of K_{ep} is the best indicator for distinguishing malignant and benign lesions in quantitative DCE-MRI. For all images studied with the mp-MRI, principal component analysis and orthogonal partial least squares discriminant analysis (OPLS-DA) revealed a clear difference between tumor and healthy regions in the peripheral zone. When first and second order statistics were merged, the prediction ability of the OPLS-DA models improved for all picture modalities [24].

Previous studies usually use the average of PKP to assay the perfusion or permeability of the lesions [20-23]. However, it is well known that due to the heterogeneity of prostate lesion signal intensity, especially in the central gland, prostate cancer and BPH have overlapping images [12]. To address such problem, there have been limited studies of WAHPP used in prostate. Bao *et al.* suggested that histogram analysis could help the differentiation of prostate cancer lesions with DWI [25]. Similarly, Zhang *et al.* indicated that the histogram metrics of IVIM parameters were related to Gleason grade of prostate cancer. However, there were few reports on the superiority of histogram analysis for WHAPP in prostate lesions [26]. Because most metrics can distinguish between benign and malignant tissues

[DOI: 10.52547/ijrr.20.2.34]

with a ROI of 10 mm, Lai *et al.* confirmed that ROI 10 mm is the most acceptable size [27].

The WHAPP of the DCE-MRI obtained from malignant prostate lesions differed considerably from benign lesions in this investigation. The histological features of malignant tumors can explain this result. Tumor arteries in malignant lesions are more diverse in size and disordered than those in benign lesions. For example, in the aspect of histogram parameters, entropy is a measure of textural irregularity that shows how close an image is to a uniform distribution of grey levels. Increased heterogeneity is indicated by higher entropy and poorer homogeneity [28, 29]. As was showed in our results, the entropy of PCa exhibited the higher entropies of K^{trans}, K_{ep} and V_p, which corroborated the theory that malignant tumors are more heterogeneous. The asymmetry of a real-valued random variable's probability distribution can be calculated by Skewness a histogram [28]. The PCa-V_p skewness was lower than that of the benign lesions, suggesting that more pixels have higher V_p value, thus shift the histogram to the right side.

Furthermore, combined histogram metrics by using multivariate logistic regression showed an improved diagnostic performance for discriminating PCa and BPH. AUC analysis suggested that K^{trans}-5th percentile (0.698), K_{ep}- Quantile 90, (0.764), V_e-uniformity (0.699) and V_p-Energy (0.729) were the most representative parameters in the redundant data, but their AUC values were less than 0.80. This indicates that TPR and FPR still need to be taken into account in the differential diagnosis of PCa, and therefore it is recommended that the clinical introduction of these parameters should be combined with other tests for a comprehensive analysis.

Our study also had some limitations: 1. DCE-MRI mainly thought scan the target lesions repeated continuously to get the origin images, the results of WAHPP from a continuous ROIs were delineated by hand slice-by-slice; 2. DCE-MRI needs a high time resolution which decreased the spatial resolution of the image, resulting in unclear lesion marge to draw the contour accurately, it is impossible to avoid the bias and error of the study.

CONCLUSION

The available indicators for quantitative prostate DCE-MRI include WHAPP-K^{trans}, K_{ep} and V_e, of which Kep-Quantile 90 may be the most excellent predictor to distinguish malignant from BPH.

ACKNOWLEDGMENTS

Not applicable.

***Ethics approval and consent to participate*:** This study was approved by the Ethics Committee of Gansu Provincial Hospital [2016-089].

***Conflict of Interest*:** *Declared none.*

***Funding*:** Gansu Province Hospital ,Research Fund, No.20GSSY1-18.

***Authors' contributions*:** guarantor of integrity of the entire study: Gang Huang, Lian-ping Zhao2 study concepts and design:Gang Huang, Xiao-mei Ma, Li-li Wang. literature research:Xiao-mei Ma, Li-li Wang, Jian-wei He. clinical studies:Xiao-mei Ma, Lili Wang,Ya-qiong Ma ,Wen-wen Zhang. experimental studies :Xiao-mei Ma, Ping Wang, Jian-wei He. data analysis:Xiao-mei Ma Li-li Wang, Jia-liang Ren. statistical analysis: Xiao-mei Ma, Jia-liang Ren, Zhong-qiang Shi. manuscript preparation:Xiao-mei Ma. manuscript editing:Xiao-mei Ma, Li-li Wang. manuscrip modification: Li-li Wang, Jia-liang Ren, Zhong-qiang Shi. All authors read and approved the final manuscript.

REFERENCES

1. Torre LA, Bray F, Siegel RL, Ferlay J, Lortet-Tieulent J, Jemal A (2015) Global cancer statistics, 2012. *CA Cancer J Clin, **65**: 87-108*.
2. Roddam AW, Duffy MJ, Hamdy FC, Ward AM, Patnick J, Price CP, Rimmer J, Sturgeon C, White P, Allen NE; NHS Prostate Cancer Risk Management Programme. (2005) Use of prostate-specific antigen (PSA) isoforms for the detection of prostate cancer in men with a PSA level of 2-10 ng/ml: systematic review and meta-analysis. *Eur Urol, **48**: 386-399*.
3. De Nunzio C, Kramer G, Marberger M, Montironi R, Nelson W, Schröder F, Sciarra A, Tubaro A (2011) The controversial relationship between benign prostatic hyperplasia and prostate cancer: the role of inflammation. *European Urology, **60**(1): 106-17*.
4. Niu XK, Chen ZF, Chen L, Li J, Peng T, Li X (2018) Clinical Application of Biparametric MRI Texture Analysis for Detection and Evaluation of High-Grade Prostate Cancer in Zone-Specific Regions. *AJR Am J Roentgenol, **210**(3): 549-556*.
5. Pagano F, Zattoni F, Vianello F, Piazza R, Capitanio G (1991) Is there a relationship between benign prostatic hyperplasia and prostatic cancer? *Eur Urol, **20**(1) 31-35*.
6. Bostwick DG, Cooner WH, Denis L, Jones GW, Scardino PT, Murphy GP (1992) The association of benign prostatic hyperplasia and cancer of the prostate. *Cancer, **70**: 291-301*.
7. Macefield RC, Metcalfe C, Lane JA, Donovan JL, Avery KN, Blazeby JM, Down L, Neal DE, Hamdy FC, Vedhara K, Protect Study Group (2010) Impact of prostate cancer testing: an evaluation of the emotional consequences of a negative biopsy result. *Br J Cancer, **102**: 1335-1340*.
8. Hambrock T, Somford DM, Hoeks C, Bouwense SA, Huisman H, Yakar D, van Oort IM, Witjes JA, Fütterer JJ, Barentsz JO (2010) Magnetic Resonance Imaging Guided Prostate Biopsy in Men With Repeat Negative Biopsies and Increased Prostate Specific Antigen. *J Urol, **183**: 520-8*.
9. Rais-Bahrami S, Siddiqui MM, Vourganti S, Turkbey B, Rastinehad AR, Stamatakis L, Truong H, Walton-Diaz A, Hoang AN, Nix JW, Merino MJ, Wood BJ, Simon RM, Choyke PL, Pinto PA (2015) Diagnostic value of biparametric magnetic resonance imaging (MRI) as an adjunct to prostate specific antigen (PSA)-based detection of prostate cancer in men without prior biopsies. *BJU Int, **115**: 381-388*.
10. Stanzione A, Imbriaco M, Cocozza S, Fusco F, Rusconi G, Nappi C, Mirone V, Mangiapia F, Brunetti A, Ragozzino A, Longo N (2016) Biparametric 3T magnetic resonance imaging for prostatic cancer detection in a biopsy-naïve patient population: a further improvement of PI-RADSv2? *Eur J Radiol, **l85**: 2269-2274*.
11. Cho E, Chung DJ, Yeo DM, Sohn D, Son Y, Kim T, Hahn ST (2015) Optimal cut-off value of perfusion parameters for diagnosing prostate cancer and for aggressiveness associated with Gleason score. *Clin Imaging, **39**(5): 834-840*.
12. Verma S, Turkbey B, Muradyan N, Rajesh A, Cornud F, Haider MA, Choyke PL, Harisinghani M (2012) Overview of Dynamic Contrast-

[DOI: 10.52547/ijrr.20.2.34]

Enhanced MRI in Prostate Cancer Diagnosis and Management. *AJR Am J Roentgenol,* ***198****(6): 1277-88*.
13. Cirkel GA, Gadellaa-van Hooijdonk CG, Koudijs MJ, Willems SM, Voest EE (2014) Tumor Heterogeneity and Personalized Medicine， are we being outnumbered? *Future Oncol,* ***10****(3): 417-28.*
14. Li Z, Ai T, Hu Y, Yan X, Nickel MD, Xu X, Xia L (2018) Application of whole-lesion histogram analysis of pharmacokinetic parameters in dynamic contrast-enhanced MRI of breast lesions with the CAIPIRINHA-Dixon-TWIST-VIBE technique. *J Magn Reson Imaging,* ***47****(1): 91-96*.
15. Donati OF, Mazaheri Y, Afaq A, Vargas HA, Zheng J, Moskowitz CS, Hricak H, Akin O (2014) Prostate Cancer Aggressiveness: Assessment with Whole-Lesion Histogram Analysis of the Apparent Diffusion Coefficient. *Radiology,* ***271****(1): 143-52*.
16. Cui Y, Yang X, Du X, Zhuo Z, Xin L, Cheng X. (2018) Whole-tumour diffusion kurtosis MR imaging histogram analysis of rectal adenocarcinoma: Correlation with clinical pathologic prognostic factors. Eur Radiology. 4, 1485-1494.
17. Schaefer JF, Vollmar J, Schick F, Vonthein R, Seemann MD, Aebert H, Dierkesmann R, Friedel G, Claussen CD (2004) Solitary pulmonary nodules: dynamic contrast enhanced MR imaging-perfusion differences in malignant and benign lesions. *Radiology,* ***232****(2): 544-553*.
18. Engelbrecht MR, Huisman HJ, Laheij RJ, Jager GJ, van Leenders GJ, Hulsbergen-Van De Kaa CA, de la Rosette JJ, Blickman JG, Barentsz JO (2003) Discrimination of prostate cancer from normal peripheral zone and central gland tissue by using dynamic contrast-enhanced MR imaging. *Radiology,* ***229****(1): 248-54*.
19. Girouin N, Mège-Lechevallier F, Tonina Senes A, Bissery A, Rabilloud M, Maréchal JM, Colombel M, Lyonnet D, Rouvière O (2007) Prostate dynamic contrast-enhanced MRI with simple visual diagnostic criteria: is it reasonable? *Eur Radiol,* ***17****(6): 1498-509*.
20. Kozlowski P, Chang SD, Meng R, Mädler B, Bell R, Jones EC, Goldenberg SL (2010) Combined prostate diffusion tensor imaging and dynamic contrast enhanced MRI at 3T-quantitative correlation with biopsy. *J Magn Reson Imaging,* ***28****(5): 621-628*.
21. van Niekerk CG, van der Laak JA, Hambrock T, Huisman HJ, Witjes JA, Barentsz JO, Hulsbergen-van de Kaa CA (2014) Correlation between dynamic contrast-enhanced MRI and quantitative histopathologic microvascular parameters in organ-confined prostate cancer. *Eur Radiol,* ***24****(10): 2597-2605*.
22. Langer DL, van der Kwast TH, Evans AJ, Trachtenberg J, Wilson BC, Haider MA (2009) Prostate cancer detection with multi-parametric MRI: logistic regression analysis of quantitative T2, diffusion-weighted imaging, and dynamic contrast-enhanced MRI. *J Magn Reson Imaging,* ***30****(2): 327-334*.
23. Jackson AS, Reinsberg SA, Sohaib SA, Charles-Edwards EM, Jhavar S, Christmas TJ, Thompson AC, Bailey MJ, Corbishley CM, Fisher C, Leach MO, Dearnaley DP (2009) Dynamic contraster-damaced MRI for prostate cancer localization. *Br J Radiol,* ***82****(974): 148-156*.
24. Kuess P, Andrzejewski P, Nilsson D, Georg P, Knoth J, Susani M, Trygg J, Helbich TH, Polanec SH, Georg D, Nyholm T (2017) Association between pathology and texture features of multi parametric MRI of the prostate. *Phys Med Biol,* ***62****(19): 7833-7854*.
25. Bao J, Wang X, Hu C, Hou J, Dong F, Guo L (2017) Differentiation of prostate cancer lesions in the Transition Zone by diffusion-weighted MRI. *Eur J Radiol Open,* ***4****: 123-128*.
26. Zhang YD, Wang Q, Wu CJ, Wang XN, Zhang J, Liu H, Liu XS, Shi HB (2015) The histogram analysis of diffusion-weighted intravoxel incoherent motion (IVIM) imaging for differentiating the gleason grade of prostate cancer. *Eur Radiol,* ***25****(4): 994-1004*.
27. Lai CC, Huang PH, Wang FN, Shen SH, Wang HK, Liu HT, Chung HJ, Lin TP, Chang YH, Pan CC, Peng SL (2019) Histogram analysis of prostate cancer on dynamic contrast-enhanced magnetic resonance imaging: A preliminary study emphasizing on zonal difference. *PLoS One,* ***14****(2): e0212092*.
28. Yoon SH, Park CM, Park SJ, Yoon JH, Hahn S, Goo JM (2016) Tumor heterogeneity in lung cancer: Assessment with dynamic contrast-enhanced MR imaging. *Radiology,* ***280****(3): 940-8*.
29. Win T, Miles KA, Janes SM, Ganeshan B, Shastry M, Endozo R, Meagher M, Shortman RI, Wan S, Kayani I, Ell PJ, Groves AM (2013) Tumor heterogeneity and permeability as measured on the CT component of PET/CT predict survival in patients with non-small cell lung cancer. *Clin Cancer Res,* ***19****(13): 3591-3599*.

[DOI: 10.52547/ijrr.20.2.34]